SRIM simulation of irradiation damage by protons in ZnO:S compound

A. Y. Boboev [a,*], N. Y. Yunusaliyev [a], G. G. Tojiboyev [a], O. Shk. Muminov [a], S. R. Kadirov [b]
[a] *Andijan state university named after Z.M. Babur, Andijan, Uzbekistan*
[b] *Urgench state university,Urgench city, Uzbekistan*

In this paper, using the Stopping and Range of Ions in Matter (SRIM) simulation, we considered the case of irradiating sulfur doped zinc oxide (ZnO:S). The composition in the study was 48.0% Zn, 49.0% O, and 3.0% S, and we analyzed the implications of various proton energies (10 keV, 100 keV, 500 keV and 1000 keV). Our analyses examined the depth profile of vacancy concentration, ionization, phonon energy loss, and recoil energies of the sputtered material. Results show that the higher concentration of vacancies generated near the surface when irradiated with low energy protons (10–100 keV) and the deeper penetration of the high energy protons (500–1000 keV), that generates a more homogeneous ionization. Additionally, the modest energy loss on the material is attributable to the ionization involving the higher energy protons, because these form the basis of the ionizing particle. The results provide a scientific basis for making ZnO-based device designs radiation-resistant.

(Received September 9, 2025; Accepted December 4, 2025)

Keywords: Proton irradiation, SRIM simulation, Electronic stopping power, Nuclear stopping power, Ionization energy loss, Vacancy formation, DPA(displacements per atom), Projected range, Radiation damage

1. Introduction

In the field of modern technological development, the issue of radiation resistance of semiconductor materials has become one of the pressing fields of scientific research. Precisely, the stability of the devices used in micro- and nanoelectronics, optoelectronic devices [1], radiation sensors [2], and the nuclear power sector directly determines the reliability of these devices in radiation conditions [3]. Therefore, there is a growing need for thorough examination of the radiation-induced defect creation mechanisms—recombination centers, vacancies, and dislocations—present in materials [4].

Transparent conductive oxides (TCO), particularly zinc oxide (ZnO), have attracted widespread attention in the last few years due to their unusual physical and chemical properties. These compounds possess high optical transparence in the visible spectra range and high electrical conductivity, which makes them good options for devices in optoelectronics, sensors, transparent electrodes, and radiation-hardened electronics. Among the group of metal oxide semiconductors, sulfur-doped ZnO thin films are suitable options for radiation-hardened electronics due to the fact that they can be tailored with their bandgap, are stable chemically, and are low-cost to produce using processes such as sol-gel and ultrasonic spray pyrolysis [5,6]. Since the devices made from these materials are designed to operate in radiation-rich environments, the determination of initial radiation damage and proton-induced ion–matter interaction is a significant task awaiting accomplishment. During this research work, the initial proton irradiation-induced damage in ZnO:S thin films was approximated by the Ion Distribution and Quick Calculation of Damage (Q-C) mode of SRIM (Stopping and Range of Ions in Matter) software. Simulations were conducted based on depth-resolved damage analysis using the output data from the VACANCY.txt, IONIZ.txt, and PHONON.txt files [7]. Calculations based on results from the Q-C methodology allowed calculation of distribution of ionization-induced and nuclear-collision-induced defects over an extended proton

* Corresponding authors: aboboyevscp@gmail.com
https://doi.org/10.15251/JOR.2025.216.781

energy range (10 keV to 1 MeV). Proton trajectories and the simulated damage profiles following SRIM's statistical binary collision approximation (Binary Collision Approximation – BCA) were thoroughly examined in the course of research. These outcomes are of highly significant significance in determining radiation hardness of ZnO:S material, sensor device operation for optimization, and semiconductor radiation-hardened structure design.

2. Materials and methods

2.1. SRIM simulation program (for ZnO:S target under proton irradiation)

SRIM (Stopping and Range of Ions in Matter) is a type of Monte Carlo ion transport simulation program that models interactions between energetic ions and solid targets. It is commonly used in radiation effects studies to predict ion penetration depth, energy loss, vacancy formation, and atomic displacements with a wide variety of materials. In this study, as noted in reference [8], the response of sulfur-doped ZnO (ZnO:S) metal oxide thin films—with an atomic composition of 48.0% Zn, 49.0% O, and 3.0% S—to proton irradiation was modeled and analyzed using the SRIM (Stopping and Range of Ions in Matter) simulation program. The range of energies for the incident protons was from 10 keV to 1000 keV to measure shallow (<1μm) surface effects and deep penetration behavior. SRIM contains two main modules: Stopping and Range of Ions in Matter (SR), which quickly produces stopping power and range tables for selected ion-target combinations, and Transport of Ions in Matter (TRIM), which models the details of the millions of collision events that occur between the incoming ions and the target atoms. In TRIM, the output data can include ion range distributions, ionization energy loss, phonon energy loss, recoil distributions, and point defect generation such as vacancy and interstitials [9]. In the simulation, the atomic numbers of the incident proton ($Z_1 = 1$), and the different target atoms (Zn = 30; O = 8; S = 16) are defined. The incident ion energy E, is dispersed as it undergoes a chain of binary collisions with target atoms which results in energy distributions, E_1 to the ion and E_2 to the target atom. Each of these energies can be further categorised based on the displacement threshold energy, E_{disp} (for ZnO, the energy ranges from 25–40 eV depending on crystal orientation). The major outcomes may be described using the following: If $E_2 >$ E disp and the subsequent target atom (displaced/primary knock-on atom, PKA) has "enough" energy to leave the lattice site and form thus, has displaced; If $E_2 > E_{disp}$ and $E_1 > E_{disp}$, then both the target and ion, can each undergo subsequent collision and produce cascade displacement events and subsequently produce multiple point defects (i.e., Frenkel pairs); If $E_2 < E_{disp}$ and $E_1 < E_{disp}$, then both target and the incident, do not displace, and instead, both dispersions dissipate as phonons and subsequently create localized heating of the lattice; If $E_2 > E_{disp}$ and $E_1 < E_{disp}$, both substitution or interstitials could occur, but this varies, if $Z_1 = Z_2$. (Remember for protons $Z_1 \neq Z_2$) the result is, the incident ion is generally an interstitial hydrogen defect. During these collisions, both elastic collisions (nuclear stopping) and inelastic collisions (electronic stopping) contribute to the total energy loss. In the case of ZnO:S, the SRIM results indicated that at low proton energies (~10-100 keV), nuclear stopping is expected to prevail, resulting in a high density of point defects close to the surface. Maximum recoil energies and number of recoils was substantially higher at low energies, however, at higher energies (~500-1000 keV) electronic stopping becomes increasingly important, with protons penetrating up to ~3000 Å but with low recoil energies and damage per ion. The simulation indicated that ionsionization energy loss increases as the proton energy increases such that at 1 MeV, about 99% of the total energy lost was due to ionization energy loss, whereas had a maximum phonon energy loss of 1 keV/ion in all cases. The maximum theoretical vacancy depths increased from ~1000 Å at 10 keV to nearly 2900 Å at 1 MeV, confirming the transition from surface to bulk damage regime is gradual and continuous. These results provide valuable insight into the nature of defect generation in ZnO-based devices exposed to space or radiation environments [10].

3. Results and discussion

3.1. Energy loss in ZnO:S at different proton energies

As shown in Table 1, we used the SR module of the SRIM simulation package to calculate the electronic and nuclear stopping power, and ultimately the projected range, of protons on ZnO:S (sulfur doped zinc oxide) at different energies. The total stopping power is the energy loss rate per unit path length of the proton as it travels through the target material and consists of two independent contributions: electronic stopping power $(-dE/dx)_e$ (due to the interactions with the electron cloud) and nuclear stopping power $(-dE/dx)_n$ (due to elastic collisions with the atomic nuclei of the target atoms (Zn, O, and S). As shown in our results, electronic stopping power is much larger than nuclear stopping power at all energies.

Table 1. Project Range and Stopping Power at a Different Proton Energy.

Energy (keV)	Electronic (dE/dx) [keV/μm]	Nuclear (dE/dx) [keV/μm]	Projected Range (μm)
10	93.0	4.5	0.1196
20	120.0	3.1	0.17
30	145.0	2.4	0.22
40	165.0	1.9	0.28
50	180.0	1.6	0.34
60	190.0	1.4	0.42
70	198.0	1.2	0.50
80	203.0	1.05	0.59
90	208.0	0.95	0.67
100	212.0	0.88	0.75
200	185.0	0.53	1.60
300	160.0	0.37	2.40
400	140.0	0.28	3.30
500	120.0	0.21	4.47
600	110.0	0.18	5.70
700	102.0	0.16	7.00
800	95.0	0.14	8.50
900	89.0	0.12	10.10
1000	84.0	0.10	12.00

For instance, at 10 keV, the electronic stopping is about 93 keV/um and the nuclear stopping is about 4.5 keV/μm. Beyond 10 keV, as the proton energy is increased from 10 keV to higher levels, the electronic stopping power will increase, peaking around 212 keV/μm at 100-keV, but will then slowly decrease until reaching a stable value of approximately 84 keV/um at 1 MeV. Similarly, the nuclear stopping power will consistently decrease from 4.5 keV/μm at 10 keV to 0.10 keV/μm at 1 MeV, indicating that nuclear interactions will play an increasingly diminished role as the incident energy increases [11]. These trends are charted in, with both of the stopping power components plotted as a function of proton energy. The stark difference between electronic and nuclear stopping is illuminating in terms of the nature of the energy transfer mechanisms in ZnO:S. At low energies protons deposit energy in a more efficient manner through direct collisions with nuclei, so nuclear stopping is more impactful as the protons are able to displace atoms and create defects. At higher energies the protons travel faster, and while they certainly do collide with atomic nuclei, they primarily interact with the electron cloud which leads to increased ionization and less angular scattering which results in less atomic displacement. The loss of energy to ionization represents the energy that is lost from fast protons to the bound electrons within the target atoms resulting in excitation or ejection. Eventually this energy will be dissipated as heat or phonons which are quantized atomic vibrations within the crystal lattice. Phonon energy loss exists at all energies, but

is relatively insignificant compared to ionization loss and becomes an even smaller part of loss as energy increases. According to the TRIM results, ionization energy loss makes up over 97 % of the total proton energy at all energies considered: 0.009 keV/ion at 10 keV and 999.3 keV/ion at 1 MeV. Phonon energy loss stays low all the time, peaking at 0.7 keV/ion at the maximum energy, which is less than 3 % of the total [12].

As shown in Figure 1, the 3D visualizations of energy loss showed that protons of an energy of 1 MeV lack spatial directionality when dissipating energy through the ZnO:S lattice as they lose energy losing most energy through electronic stopping along a pathway of relatively straight-line course.

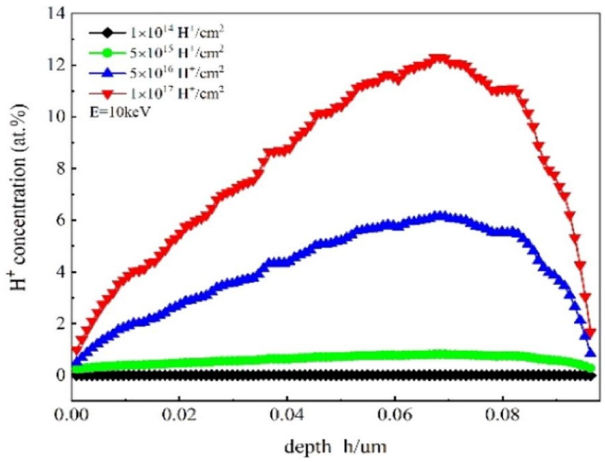

Fig. 1. H^+ Concentration in ZnO:S at different fluences (10 kev); peaks around 0.04–0.05 μm depth.

Fig 2 (a) and Fig 2 (b) also shows a characterisation of ionization loss and energy lost via phonons as a function of proton energy. The data shows quite clear evidence that while increasing incident energy increases total ionization loss, the amount of energy lost into phonons is decreasing incrementally suggest a better efficiency of energy transport with less disturbance to the lattice with increasing energy. The employed behavior can also help explain why vacancy production is increasing with energy, but at decreasing increments, since protons are collecting fewer atoms to displace in collisions with heavier nuclei. Based on the data presented here, the energy loss behavior for protons in ZnO:S is conditionally said to be dominated by electronic interactions in the energy range studied, with significant contributions to nuclear effects only at low energies. This has immediate implications within radiation-induced defect engineering studies. The implication is quite simple, that low energy protons are more effective for producing localized structural damage to materials, while high energy protons resulted primarily in ionization that tended not to disrupt the atomic lattice [13].

3.2. Vacancies in ZnO:S under proton irradiation

When protons collide with an atom (Zn, O, or S) with sufficient energy, they collide elastically and displace the atom from its original lattice site, causing a primary displacement event. The displaced atom may produce a cascade of secondary collisions, creating defects after the cascade and leaving behind a vacancy. In ZnO:S, Zn vacancies act as scattering centers, carrier traps, or recombination centers [14]. When vacancies act as recombination centers, they effectively reduce the minority carrier lifetime; as traps, they decrease free carrier concentration (increasing the number of carriers establishing traps); overall, the defects decrease mobility which increases the number of phonon and impurity scattering mechanisms [15]. The vacancy distribution with depth indicates that low-energy protons cause damage primarily at or very near the surface (~1000–1200 Å at 10–100 keV), whereas high-energy protons penetrate deeper and distribute damage more broadly (~3000 Å at 1 MeV). However, even though the high-energy protons penetrate deeper, the vacancy density is less at depth because of reduced nuclear stopping.

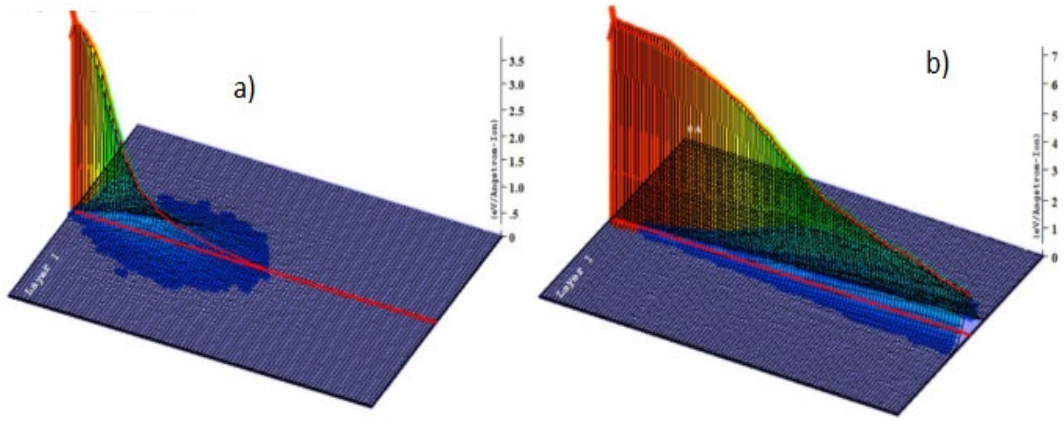

Fig. 2. 3D View of proton energy loss in ZnO:S: (A) high-energy protons penetrate deeply with energy loss dominated by electronic stopping; (B) Low-energy protons deposit. Energy near the surface with prominent nuclear stopping and localized damage.

The simulated vacancy profiles presented in Figure 3 illustrate this behavior, as a function of depth, across varying angles and energies of protons. As the angle of incidence increases, the effective path length of the proton through the material also increases, which results in broad distribution depth and moving the peak of the vacancy concentration closer to the surface. The deepest occurring vacancy concentration and most sporadic concentration occurs at normal incidence, while the most localized and surface concentrations occur at angles ≥ 45°. Ultimately, the simulation supports that vacancy generation in ZnO:S depends strongly on proton energy and incidence geometry. Low energy protons (below 100 keV) deliver concentrated surface damage due to favorable nuclear interactions; however, higher energy protons deliver distributed but softened damage deeper in the lattice due to the amount of energy lost through ionization rather than nuclear interactions. This information is useful when optimizing performances of ZnO:S material in regimes where radiation tolerance and defect control are important: space-based sensors, radiation detectors, and oxide electronics [16].

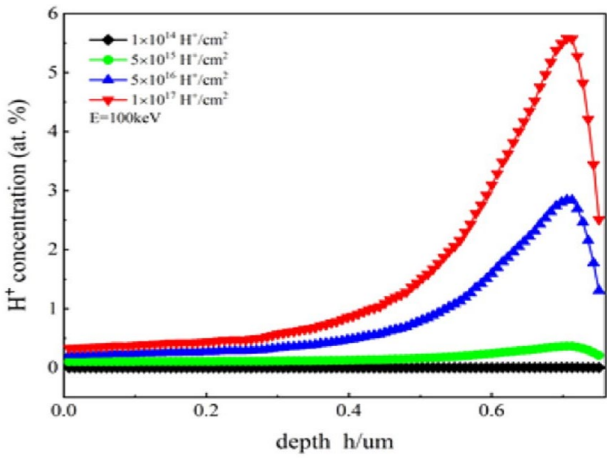

Fig. 3. H^+ Concentration in ZnO:S at various fluences (100 kev); peaks at ~0.6 μm depth.

3.3. Variation of vacancy concentration with irradiation fluence in ZnO:S at different proton energies

While the TRIM simulation is telling us the distribution of ion-induced displacements as a function of depth, the output is relative units only and must be converted into real physical quantities with irradiation fluence. In order to obtain the real vacancy concentration profile for realistic scenarios, we simply use the following relation:

$$DPA = \frac{F \cdot R}{N_0} \tag{6}$$

where R is the concentration of irradiation induced vacancies (atoms/cm³), F is the irradiation fluence (ions/cm²), and N_0 is the atomic number density of ZnO:S, which is calculated to be around $4.1 \cdot 10^{22}$ atoms/cm³ based on composition and density. Using this equation, concentration profiles for vacancies were determined at each energy level (10 keV, 100 keV, 500 keV, and 1 MeV) for four fluence values: $1 \cdot 10^{14}$, $5 \cdot 10^{15}$, $5 \cdot 10^{16}$, and $1 \cdot 10^{17}$ ions/cm². All four energies were chosen to represent a different regime of damage: surface-localized protons to deep-penetrating protons. The depth of penetration for 10 keV protons is around 1196 Å (~0.12 μm); this is a small penetration depth and a high nuclear stopping power, which results in a highly localized vacancy distribution very near the surface with a sharp peak in concentration [17]. At high fluences on the order of $5 \cdot 10^{16}$ ions/cm² vacancy concentrations exceed 6 atoms/cm³ yielding a concentrated area of atomic displacements in the top 1000 Å of the ZnO:S layer. The total energy deposition is also larger at 100 keV versus 10 keV but vacancy concentrations peak at about 3 atoms/cm³. Although nuclear stopping power is still more dominant than electronic stopping power at this energy, it spreads out vacancy production effects. At 500 keV the proton range is about 4.67 μm. The contribution from nuclear stopping power becomes much less significant than electronic power, thus the activity for displacement is significantly less, with a peak vacancy concentration even lower at ~0.7 atoms/cm³, and the damage profile short and nearly flat over several microns in depth with long uniform tails in the distribution. Protons at 1 MeV have penetration rates of ~12 μm, however because the nuclear stopping power is very low (~0.08 keV/μm) and ionization effects dominate, the vacancy concentration is < 0.6 atoms/cm³. Despite the increased range, the interaction cross-section with lattice atoms is quite small, which greatly reduces the efficiency of vacancy production. With increasing protons fluence of $1 \cdot 10^{14}$ to $1 \cdot 10^{17}$ ions/cm², the concentration of vacancies grows linearly; however, the shape and depth of the overall damage profile is primarily a function of the incident proton's energy. At very high fluences ($5 \cdot 10^{16}$ ions/cm², the difference between the low- and high-energies become clearer [18]: low-energy protons produced a sharp and dense vacancy concentration near the surface, but high-energy protons produced broader, more dilute damage profiles in greater depths in the target. In conclusion, the proton energy and fluence must be carefully rationalized depending on the desired depth of modification. For surface modifications and defect engineering, low-energies, high-fluence bombardment are ideal. In contrast, higher energies are preferable where bulk integrity should be maintained or low defect concentrations are required for definitive applications [19].

3.4. Variation of DPA with irradiation fluence at different proton energies

In highly radiative environments, such as in space or nuclear environments, the energy spectrum and flux of incident charged particles can vary greatly and unpredictably. These high energy particles can cause considerable irradiation damage that can degrade both the electrical and structural properties of semiconductor materials, such as ZnO:S. Irradiation damage can result in threshold voltage shifts, increased leakage currents, and complete device failure in the worst case. To quantify the specific effect of irradiation damage, we calculated the displacement per atom (DPA) in ZnO:S using SRIM/TRIM simulations and the standard DPA calculation [20]:

$$DPA = \frac{F \cdot R}{N_0} \tag{1}$$

where F is the irradiation fluence in ions/Å², R is the number of displacements per ion per unit depth (derived from vacancy.txt in TRIM), and N_0 is the atomic number density of ZnO:S was estimated

at an atomic number density of approximately $4.1 \cdot 10^{-2}$ atoms/Å^3 or $4.1 \cdot 10^{22}$ atoms/cm^3. Using this equation, we calculated depth-dependent DPA distributions at four representative proton energies, 10 keV, 100 keV, 500 keV, and 1 MeV, and at multiple fluence values: $1 \cdot 10^{14}$, $5 \cdot 10^{15}$, $5 \cdot 10^{16}$, and $1 \cdot 10^{17}$ ions/cm^2 [21]. The resulting DPA profiles are displayed in 14. At 10 keV, DPA is peaked near the surface (~0.12 μm) with recoil energy of approximately 0.2 eV/Å. The high energy transfer to lattice atoms results in a concentrated amount of displacement activity, yielding a peak DPA of ~0.5 at fluence $5 \cdot 10^{16}$ ions/cm^2. However, at this shallow depth, everything below it is lost deposition due to an extremely short projected range of low-energy protons. DPA decreases quite rapidly with depth. At 100 keV the projected range has increased to ~0.75 μm and the DPA distribution is consequently broader. The peak DPA decreases to ~0.3 to 0.35 meaning that the damage profile is more dispersed. This is attributed to at least one of the effects described previously having balanced nuclear stopping and lower recoil energy density over a larger volume. For the 500 keV protons, maximum DPA drops further to ~0.15, while the damage depth increases significantly to ~4.67 μm. At this energy, nuclear stopping continues to be less than at lower energy and displacements are dispersed more evenly throughout the volume. At 1 MeV, the depth of damage is a little deeper (~12 μm) with the lowest peak DPA (~0.10-0.12). This low peak DPA means that the efficiency of high-energy protons displacing lattice atoms is reduced due to less nuclear interaction and more electronic stopping [22]. The higher total incident energy still generates only rather small displacements because of lack of adequate momentum transfer. In general, the simulation-determined DPA results decrease as the proton energy increases because of the shifting energy loss mechanisms from nuclear stopping to electronic stopping. Low-energy protons are far better than high-energy protons to transfer energy to the lattice to generate a displacement/ vacancy. High energy protons, on the other hand, perform the same ionization processes as lower energy protons but don't impart sufficient kinetic energy to generate atomic displacement. However, absolute values of DPA scales linearly with fluence, but both the shape and depth of the damage profile depend significantly on the proton energy. These findings provide a perspective on the trade-offs associated with selection of irradiation energy and fluence for both very damaging and potentially beneficial radiation effects in the context of designing ZnO:S based devices for radiation environments where the full operational life might include high fluence levels or low-grade doses in low-energy proton environments. Ideally, low-energy and high-fluence protons will induce locally controllable damage near the surface. High-energy protons are more suited for radiation applications where deep penetration is necessary while avoiding lingering structure [23].

4. Conclusions

The results showed that the electronic stopping power was significantly higher than the nuclear stopping power at all tested energy levels, with more than 97% of the total energy loss resulting from ionization. Low-energy protons (10–100 keV) caused not only a high density of vacancies near the ZnO surface but also relatively dense defect formation due to increased nuclear stopping. In contrast, high-energy protons (500 keV–1 MeV) caused less damage to the sample but penetrated deeper into the material. The radiation-induced damage was relatively mild because most of the proton energy was dissipated through ionization rather than direct atomic displacements. The DPA (displacements per atom) values sharply decreased with increasing proton energy, indicating that low-energy protons caused significantly higher damage. However, as energy increased, the extent of damage decreased while reaching deeper layers.

Based on our findings, we propose that low-energy proton irradiation is a suitable method for surface modification or tuning of materials, whereas high-energy protons can be effectively used to alter the bulk of the material without disrupting or destructively modifying the crystal structure. The data presented in our study provide a scientific basis for designing ZnO-based devices suitable for use in radiation-intensive environments such as space technologies, optoelectronic sensing, and nuclear instrumentation.

References

[1] Y. Lee, H.-W. Lee, S. Park, J. Kim, J. Lee, Nano Convergence, 12(1), 1–9 (2025); https://doi.org/10.1038/s41427-025-00234-2
[2] S. Z. Zainabidinov, A. Y. Boboev, N. Y. Yunusaliyev, B. D. Gulomov, J. A. Urinboyev, East European Journal of Physics, 4, 443–446 (2024); https://doi.org/10.26565/2312-4334-2024-4-53
[3] M. S. Qureshi, K. Zeng, D. Xiang, Materials Science in Semiconductor Processing, 173, 1–24 (2024); https://doi.org/10.1016/j.mssp.2024.107654
[4] A. Y. Boboev, B. M. Ergashev, N. Y. Yunusaliyev, M. M. Xotamov, East European Journal of Physics, 2, 292–296 (2025); https://doi.org/10.26565/2312-4334-2025-2-36
[5] P. Abraham, S. Shaji, D. A. Avellaneda, J. A. Aguilar-Martínez, B. Krishnan, Materials Today Communications, 35, 105909 (2023); https://doi.org/10.1016/j.mtcomm.2023.105909
[6] S. Z. Zainabidinov, A. Y. Boboev, N. Y. Yunusaliyev, J. N. Usmonov, East European Journal of Physics, 3, 293–300 (2024); https://doi.org/10.26565/2312-4334-2024-3-53
[7] M. Titze, J. L. Pacheco, T. Byers, S. B. Van Deusen, D. L. Perry, D. Weathers, E. S. Bielejec, Journal of Vacuum Science & Technology A, 39(6), 063222 (2021); https://doi.org/10.1116/6.0001287
[8] A. Y. Boboev, X. A. Maxmudov, N. Y. Yunusaliyev, B. M. Ergashev, G. G. Tojiboyev, F. A. Abdulkhaev, Journal of Ovonic Research, 21(4), 481–493 (2025); https://doi.org/10.15251/JOR.2025.214.481
[9] U. Kutliev, M. Karimov, B. Sadullaeva, and M. Otaboev, COMPUSOFT: An International Journal of Advanced Computer Technology, 7(4), 2749–2751 (2018); https://ijact.in/index.php/j/article/view/431/412
[10] I. Ayoub, V. Kumar, M. A. Alshahrie, et al., Nanotechnology Reviews, 11(1), 575–619 (2022); https://doi.org/10.1515/ntrev-2022-0035
[11] P. Kumari, A. Srivastava, R. K. Sharma, A. Saini, D. Sharma, J. S. Tawale, S. K. Srivastava, Materials Today Communications, 32, 103845 (2022); https://doi.org/10.1016/j.mtcomm.2022.103845
[12] H. M. Qadr, A. M. Hamad, RENSIT, 12(4), 451–456 (2020); https://doi.org/10.17725/rensit.2020.12.451
[13] G. Nandipati, W. Setyawan, K. Roche, R. J. Kurtz, H. L. Heinisch, Journal of Nuclear Materials, 542A, 152402 (2020); https://doi.org/10.1016/j.jnucmat.2020.152402
[14] A. Y. Boboev, K. A. Makhmudov, Z. M. Ibrokhimov, A. K. Rafikov, N. Y. Yunusaliyev, S. K. Ibrokhimov, East European Journal of Physics, 2, 436–440 (2025); https://doi.org/10.26565/2312-4334-2025-2-54
[15] B. Patra, A. Das, D. Basak, Physica B: Condensed Matter, 678, 415745 (2024); https://doi.org/10.1016/j.physb.2024.415745
[16] Y. Dong, F. Tuomisto, B. G. Svensson, A. Y. Kuznetsov, L. J. Brillson, Physical Review B, 81(8), 081201 (2010); https://doi.org/10.1103/PhysRevB.81.081201
[17] R. Rasmidi, M. Duinong, F. P. Chee, Radiation Physics and Chemistry, 184, 1–10 (2021); https://doi.org/10.1016/j.radphyschem.2021.109456
[18] B. Carleer, Journal of Physics: Conference Series, 1063(1), 012001 (2018); https://doi.org/10.1088/1742-6596/1063/1/012001
[19] J. Zhou, R. Hao, X. Pan, Y. Ren, J. Li, J. Zhao, J. Kong, Journal of the Korean Physical Society, 82(4), 364–374 (2023); https://doi.org/10.1007/s40042-023-00900-4
[20] P. Pakseresht, S. V. Apte, International Journal of Multiphase Flow, 113, 16–32 (2019); https://doi.org/10.1016/j.ijmultiphaseflow.2018.12.012
[21] Z. Ali, F. Liu, Y. Wang, H. G. Rasool, F. Wang, M. Haseeb, Nuclear Engineering and Technology, 57(8), 103570 (2025); https://doi.org/10.1016/j.net.2025.103570
[22] C. Marques, F. Wrobel, Y. Aguiar, A. Michez, J. Boch, F. Saigné, R. García Alía, et al., Eng, 5(1), 319–332 (2024); https://doi.org/10.3390/eng5010021
[23] B. B. Sharma, B. Chakraborty, S. Gohil, N. Garg, AIP Advances, 13(1), 015022 (2023); https://doi.org/10.1063/5.0134567